**NASA TECHNICAL MEMORANDUM**

**NASA TM X- 73902**

NASA TM X-73902

(NASA-TM-X-73902) GEARED-ELEVATOR FLUTTER STUDY (NASA) 12 p HC $3.50 CSCL 01A

N76-28158

Unclas
G3/02 46746

# GEARED-ELEVATOR FLUTTER STUDY

Charles L. Ruhlin

Robert V. Doggett, Jr.

and

Richard A. Gregory




**NATIONAL AERONAUTICS AND SPACE ADMINISTRATION**

**LANGLEY RESEARCH CENTER, HAMPTON, VIRGINIA 23665**

| 1. Report No. | 2. Government Accession No. | 3. Recipient's Catalog No. |
|---|---|---|
| NASA TM X-73902 | | |

| 4. Title and Subtitle | 5. Report Date |
|---|---|
| GEARED-ELEVATOR FLUTTER STUDY | May 1976 |
| | 6. Performing Organization Code 2711 |

| 7. Author(s) | 8. Performing Organization Report No. |
|---|---|
| Charles L. Ruhlin, Robert V. Doggett, Jr., and Richard A. Gregory* | |
| | 10. Work Unit No. 743-01-12-01 |
| 9. Performing Organization Name and Address | 11. Contract or Grant No. |
| NASA Langley Research Center<br>Hampton, Virginia 23665 | |
| | 13. Type of Report and Period Covered Technical Memorandum |
| 12. Sponsoring Agency Name and Address | 14. Sponsoring Agency Code |
| National Aeronautics & Space Administration<br>Washington, D.C. 20546 | |

15. Supplementary Notes *Boeing Commercial Airplane Company
Technical Paper Presented at the AIAA/ASME/SAE 17th Structures, Structural Dynamics, and Materials Conference, Valley Forge, PA, May 5-7, 1976

16. Abstract

An experimental and analytical study has been made of the transonic flutter characteristics of an empennage model having an all-movable, horizontal tail with a geared elevator. Two model configurations, namely, one with a geared-elevator (2.8 to 1.0 gear ratio) and one with locked-elevator (1.0 to 1.0 gear ratio), were flutter tested in the Langley transonic dynamics tunnel with the empennage cantilever-mounted on a sting. The geared-elevator configuration fluttered experimentally at about 20% higher dynamic pressures than the locked-elevator configuration. The experimental flutter dynamic pressure boundaries for both configurations were nearly flat over a Mach number range from 0.9 to 1.1. Flutter calculations were made for the geared-elevator configuration using three subsonic lifting-surface methods. In one method, the elevator was treated as a discrete surface, and in the other two methods, the stabilizer and elevator were treated as a single warped-surface with the primary difference between these two methods being in the mathematical implementation used. Comparison of the experimental and analytical results indicated the discrete-elevator method predicted best the experimental flutter dynamic pressure level. However, the single warped-surface methods predicted more closely the experimental flutter frequencies and Mach number trends.

| 17. Key Words (Suggested by Author(s)) (STAR category underlined) | 18. Distribution Statement |
|---|---|
| Flutter<br>Transonic speeds<br>Control surface | Unclassified - Unlimited |

| 19. Security Classif. (of this report) | 20. Security Classif. (of this page) | 21. No. of Pages | 22. Price* |
|---|---|---|---|
| Unclassified | Unclassified | 7 | $3.25 |

*Available from { The National Technical Information Service, Springfield, Virginia 22151
STIF/NASA Scientific and Technical Information Facility, P.O. Box 33, College Park, MD 20740

## II. Model and Mount System

### General

Photographs of the model used in the present study are shown in Figure 2, and some dimensions and structural details are presented in Figures 3 and 4. The model was constructed, but not tested, during the National Supersonic Transport Program by The Boeing Company, and was made available by the Federal Aviation Administration for testing by the National Aeronautics and Space Administration.

The model represented a scaled version of the proposed airplane tail structure aft of the main rear wing spar, and consisted of (Fig. 2) an aft-fuselage, and vertical and horizontal tails. The horizontal-tail and aft-fuselage were geometrically, dynamically, and elastically scaled. Since symmetric flutter was of most interest, the vertical tail was made overstiff to reduce the possibility of antisymmetric flutter, but the geometric and inertia scaling were maintained. The elevator hinge gap was small but not aerodynamically sealed.

### Geometry

The horizontal tail (Fig. 3) consisted of the all-movable stabilizer and a geared, full-span elevator. Each exposed horizontal-tail panel had an aspect ratio of 0.65, a taper ratio of 0.25, and a leading-edge sweepback angle of 54°. The elevator area was about 0.25 of the total-tail area with a hinge line located at a constant 0.74 chord line (streamwise). Each exposed tail panel (excluding the carry-through structure) had a mass of about 3.4 kg (7 lbm) with a center of gravity as shown in Figure 3. The stabilizer pitch axis was located at about the 40% chordwise station of the mean aerodynamic chord. Note that the tail-panel center of gravity is aft of the pitch axis (Fig. 3).

Early in the wind-tunnel flutter tests, the sharp apex section of one tail root leading edge (about 10% of the root chord) failed under the static aerodynamic loads from the aft-fuselage downwash. This section was rebuilt as a rounded fairing (the rebuilt root chord was about 8% less than the original chord) of more substantial thickness (see Fig. 3), and, for symmetry, the other tail panel was similarly altered. All flutter data presented in this report are for this rounded apex planform.

### Construction

The model was of monocoque construction. Load-carrying webs and most skin sections were made of a sandwich-type structure formed from a lightweight, plastic foam core to which was bonded epoxy-laminated fiberglass sheets. The aft-fuselage had thin bulkheads to provide an internal frame for the skin cover. The horizontal stabilizer and vertical tail were of similar construction (Fig. 4) and employed shear and rib webs covered by and bonded to the sandwich skins. For the thinner edge sections, a lightweight foam core was used between the fiberglass skins. The elevator (Fig. 4) had a fiberglass hinge beam, a foam center core, a trailing-edge closure section of balsa, and a skin covering of multilaminated fiberglass.

The stabilizer pitch pivot (see stabilizer actuator system of Fig. 4) was mounted to a stiff fuselage bulkhead. To the pivot pin was attached a pivoting actuator arm and a bracket extending from the leading edge of the stabilizer carry-through structure. The actuator arm was driven through an articulated shaft extending from an electric drive motor located farther forward in the fuselage. The stabilizer trailing edge was also connected to the pivoting actuator arm by four steel leaf springs which simulated the stiffnesses of the four stabilizer actuators on the airplane. However, on the present model only the two inboard springs were connected to insure low symmetric flutter speeds. The arrangement shown in Figure 4 was for the elevator gear ratio of 2.8 to 1.0 (actually 2.77 to 1.0). For the ungeared model configuration (1.0 to 1.0 gear ratio), the elevator spring (Fig. 4) was replaced by a stiff fiberglass beam which locked the elevator to the stabilizer.

### Mount System

In the wind-tunnel tests, the aft-fuselage of the model was cantilevered from a long, low-frequency sting (Fig. 2) to prevent sting-body coupling in the fundamental vibration modes. An ogive nose section was attached to the forward end of the aft-fuselage in order to provide streamlined flow. The sting base was attached through pins to a massive splitter plate in the wind tunnel. The sting could be traversed vertically or pitched in the tunnel as desired by jacking screws in the splitter plate. The steel sting was very heavy. For example, the most forward sting section, which was about 3 meters long (10 ft), had a mass of over 500 kg (1100 lbm).

### Instrumentation

Model instrumentation included multiple strain-gage bridges on each stabilizer panel, strain gages and accelerometers on the fuselage, and angular position transducers on the stabilizer, elevators, and sting. This instrumentation provided dynamic response measurements of the bending and torsional deflections of the stabilizer, vertical translation, side translation, and twist of the fuselage, rotational (pitch) deflections of the stabilizer and elevators, as well as static measurements of the aerodynamic loading on the stabilizer and fuselage.

### Vibration Characteristics

Experimental. The measured node lines and frequencies associated with the symmetric natural vibration modes of each model configuration investigated are shown in Figures 5 and 6, and the measured frequencies and structural damping values (g) for these modes are presented in Table 1. In the vibration surveys, the model was excited by a single, electromechanical shaker which was located near the rear of the fuselage tail cone and provided a vertical sinusoidal force to the model. A roving accelerometer was used to trace node line patterns and determine phasing. The resonance frequencies and damping were determined by the Kennedy-Pancu method using plots of the real and imaginary parts of the ratio of model response to input force.

The nodal patterns for the two model configurations are basically similar (see Figs. 5 and 6).

However, the locked-elevator model (1.0 to 1.0 ratio) had somewhat higher frequencies. Note that the fundamental bending mode frequency of the sting was about 1.9 Hz (Table 1), and that a coupled sting-body mode was measured at about 15 Hz for both model configurations.

Calculated. The symmetric natural modes and frequencies of the 2.8 to 1.0 gear ratio configuration were calculated using a finite-element structural analysis. For this analysis, the aft fuselage was considered to be cantilevered from the streamline nose fairing. Consequently, the effects of the model being attached to the wind-tunnel sting were not included. The stabilizer and elevator were modeled using plate and beam elements; the actuators, linkages, and aft fuselage were modeled using beam elements. Initially, the structure was idealized using six substructures, namely, stabilizer, elevator, elevator linkage, inboard actuator, outboard actuator, and aft fuselage. The substructure matrices, which contained a total of 204 degrees of freedom, were merged and reduced to 125 degrees of freedom.

The first six calculated node patterns and natural frequencies are included in Figure 5. Presented in Figure 7 are isometric projections of the stabilizer-elevator portions of the mode shapes. Although the lower modes are relatively simple, being composed of varying combinations of stabilizer translation (resulting from aft fuselage bending) and pitch, and elevator rotation, considerable amounts of camber and spanwise bending are present in the higher modes.

Comparison of Experimental and Calculated Modes. The data in Figure 5 show that the calculated and measured node lines and frequencies for the 2.8 to 1.0 gear-ratio configuration are in good agreement. It was concluded that the model mode shapes were adequately described by the calculated values. Therefore, the model flutter analysis employed the calculated mode shapes and generalized masses along with the measured frequencies and damping values.

## III. Procedure

### Wind-Tunnel Flutter Tests

Test Facility. The model flutter tests were conducted in Freon-12 in the NASA Langley transonic dynamics tunnel (TDT). This facility is a return-flow, variable-pressure, slotted-throat wind tunnel which has a 4.88-m-square (16-ft) test section with cropped corners. It is capable of operation at stagnation pressures from near vacuum to slightly above atmospheric and at Mach numbers from 0 to 1.2. Mach number and dynamic pressure can be varied independently. The tunnel is equipped with four quick-opening bypass valves which can be opened to reduce rapidly the dynamic pressure and Mach number in the test section when flutter occurs.

Test Technique. During the tests, the outputs of selected model transducers were continuously recorded and visually monitored on direct readout recorders (strip charts) and magnetic tape. At operator designated points, the tunnel test conditions were digitized and printed automatically. Visual records of the model behavior were provided by high-speed motion pictures. The static loads on the horizontal tail and fuselage were visually monitored and adjustments to the stabilizer and/or sting pitch angle were made as required during the test to minimize these loads. At various test points, a real-time analyzer was used to obtain a frequency spectrum of the model response to the tunnel turbulence. During the tests these spectra were helpful in tracking various vibration modes and in observing the modal-response buildup to a flutter condition.

The usual test procedure was to select a stagnation pressure in the tunnel and slowly increase the Mach number (and dynamic pressure) until either flutter or the tunnel maximum Mach number was obtained. This procedure was repeated at consecutively higher stagnation pressures until the flutter boundary was traced over the Mach number region of interest. To insure that a near-minimum flutter speed was obtained for each model configuration tested, at least one no-flutter run was made below the flutter boundary. At flutter, the tunnel bypass valves were opened and the flutter quickly subsided. Model flutter could be easily observed from the control room. The strip charts were used primarily to measure the flutter frequency and to identify which modes were involved in the flutter.

### Flutter Analyses

General. Flutter calculations were made only for the model with an elevator-gear ratio of 2.8 to 1.0. Three methods were used to calculate the model flutter characteristics. Each method employed a modal-type analysis in which the unsteady aerodynamic forces were generated from subsonic lifting-surface (kernel function) theory.

Stabilizer With Discrete Elevator.[1] One calculation method used the kernel function procedure described in Reference 1 which allows the elevator to be treated as a surface discrete from the stabilizer and accounts for aerodynamic flow singularities at the elevator hinge line. (The hinge is aerodynamically sealed.) For these calculations, the stabilizer was treated as the main lifting surface and the elevator was treated as a trailing-edge control surface. Model flutter characteristics were calculated at Mach numbers of 0.706 and 0.872 (which matched two experimental values).

Stabilizer Elevator as Single-Warped Surface.[1] The computer program implementation of the procedure of Reference 1 is described in Reference 2. As implemented, this program[2] provides the option of treating a lifting surface without control surfaces. Flutter calculations were made using this procedure with the stabilizer and elevator treated as a single, combined surface with a warped trailing-edge region to simulate the deflected elevator. These calculations were made for Mach numbers of 0.706 and 0.872 also.

Stabilizer Elevator as Single-Warped Surface.[3] A refined kernel-function method (unpublished) based on that described in Reference 3 is in routine use for flutter calculations at NASA Langley. As in the previously discussed method, this method also treats the stabilizer and elevator as a single, combined lifting surface with a warped trailing edge. Basically, this Langley method should give results similar to those for the warped-surface

procedure of Reference 1 because the mathematical formulations of the problems are very similar with the primary differences being in the numerical implementation of the solutions. Modal flutter characteristics were calculated using this Langley method at Mach numbers of 0.706, 0.872, and 0.982.

Procedure Details. For all flutter calculations, the flow was assumed parallel to the model root chord, that is, essentially parallel to the aft-fuselage body line. For the aerodynamic model, the tip chord was rotated slightly about its midchord so that the tip chord was parallel to the root chord. The first six natural-vibration modes of the model, excluding sting-associated modes (see Fig. 5 and Table 1), were used for all calculations. The analyses employed measured frequencies with corresponding calculated mode shapes and generalized masses. Also included were the measured structural damping values for each individual mode (see Table 1). Thirty-six collocation points were used, with six points located along each chord at six spanwise stations. Surface spline functions[4] were used to interpolate the calculated modal displacements at the structural grid points to the displacements and slopes at the points required by the aerodynamic theory. For the two methods which treated the stabilizer and elevator as a single, warped surface, a single spline function was used. For the discrete-elevator method, two separate spline functions were used, one for the stabilizer and one for the elevator. The flutter equations were solved using an automated V-g solution method essentially the same as that described in Reference 5.

## IV. Results and Discussion

### Experimental Results

Symmetric flutter boundaries were determined experimentally for the model with elevator gear ratios of 2.8 to 1.0 and 1.0 to 1.0 at Mach numbers from about 0.7 to 1.14. The experimental results are compiled in Table 2 and plotted in Figure 8 as the Mach number variation of the experimental dynamic pressure required for flutter of each configuration. Included in Figure 8 are the measured frequencies at each experimental flutter point. The wind-tunnel tests were terminated when the model with 1.0 to 1.0 gear ratio was destroyed during flutter at a Mach number $M = 0.88$. From the data records, it was surmised that the left-hand structural connection between the stabilizer and elevator failed, allowing the elevator to oscillate freely, and the flutter oscillations rapidly increased until the fuselage failed and the model was destroyed.

The experimental results (Fig. 8) show that elevator gearing increased the horizontal-tail flutter dynamic pressure $q$ at transonic speeds, with the 2.8 to 1.0 elevator gear-ratio configuration having about a 20% higher flutter $q$ than the locked-elevator (1.0 to 1.0 ratio) configuration. Both model configurations had nearly flat flutter boundaries from $M = 0.9$ to 1.14. The high flutter $q$ at $M = 0.7$ for the 2.8 to 1.0 geared configuration is probably caused by variations in mass-density ratio as well as in Mach number since symmetric flutter $q$ is normally a function of mass-density ratio, especially at the relatively low mass-density-ratio values of about 3 to 10 for the present configuration. (The mass-density ratio is the ratio of tail-panel mass to the mass of the fluid enclosing the model in a volume circumscribed by rotating the tail-panel 360° in pitch about its midchord.)

The symmetric flutter mode for both model configurations was observed to be composed of aft-fuselage bending, stabilizer pitch and bending, and elevator rotation. The flutter frequencies were between the frequencies of the first two natural vibration modes of the model (identified as the fuselage vertical-bending mode and stabilizer-pitch mode).

Typical frequency spectra obtained using a real-time analyzer are presented in Figure 9. These spectra were measured during the 2.8 to 1.0 gear-ratio configuration tests, and each spectrum shows the relative amplitude of the model response to the tunnel turbulence at different $q$ levels, but all at the same $M = 0.7$. The response is that indicated by a model strain gage located to measure fuselage vertical-bending deflections. In the spectrum for the lowest $q$ (Fig. 9), several vibration modes can be identified, namely, sting fundamental bending (1.9 Hz), fuselage fundamental vertical bending (7.8 Hz), and the sting-body mode at 15.5 Hz. As $q$ increases, the fuselage bending mode gradually increases in frequency and amplitude and, although not apparent from these spectra, probably couples with a higher-frequency mode to form the flutter mode. Since the sting-associated modes remain at about the same frequencies they are evidently not involved in the flutter.

### Comparison of Analyses and Experiments

A comparison of the calculated and experimental flutter boundaries for the 2.8 to 1.0 gear-ratio configuration is presented in Figure 10 as the variations of flutter dynamic pressure and flutter frequency with Mach number. In terms of dynamic pressure (Fig. 10) the discrete-elevator method appears to agree best with experiment at $M = 0.7$, but does less well at the higher Mach numbers as both warped-surface methods follow the Mach number trend of the experiments better. The difference in numerical implementation between the warped-surface methods made a difference of about 7% in flutter $q$ levels, with the NASA Langley method[3] in closer agreement with experiment. Use of a discrete elevator rather than a warped surface considerably improved the experimental comparison for the methods based on Reference 1.

The flutter frequencies predicted by the warped-surface methods (Fig. 10) match the experimental frequencies very closely, whereas the discrete-elevator results are considerably higher than both other methods and experiment. An examination of the relative magnitudes of the generalized modal coordinates at the flutter condition for each method indicated that the calculated flutter mode shape was composed of significant contributions from the first, third, and fifth natural modes.

The reader is reminded that the calculated results were obtained by including measured structural damping values in the equations. At $M = 0.872$ some additional calculations were made with zero structural damping. These results gave an additional flutter root in the range of interest. This

root was of the "hump" type, that is, it crossed the g = 0 line in the V-g diagram, indicated an unstable range of velocity, and then recrossed the g = 0 line to the stable region. This hump was present for all three methods although the amount of penetration into the unstable region [illegible] greater for the discrete-elevator calculations a[illegible] initial crossing occurred at a lower vel[illegible] a given density. The slope of this cross[illegible] relatively small compared to the nearly ve[illegible] crossing in the V-g diagram that was used to obtain the present results (Fig. 10), and thus the present flutter mode was not very sensitive to variations in structural damping.

## V. Conclusions

An experimental and analytical study has been made of the transonic flutter characteristics of an empennage flutter model having an all-movable horizontal tail with a geared elevator. Two model configurations were flutter tested, namely, one with a geared elevator (2.8 to 1.0 gear ratio) and one with a locked elevator (1.0 to 1.0 gear ratio), with the model cantilever-mounted on a sting in the Langley transonic dynamics tunnel. Flutter calculations for the geared-elevator (2.8 to 1.0 gear ratio) configuration were made using three subsonic lifting-surface (kernel function) methods. In one, the elevator was treated as a discrete surface, and in the other two the stabilizer and elevator were treated as a single warped surface with the primary difference between these two methods being in the mathematical implementation used. All flutter calculations used the same mathematical structural model which in terms of vibration characteristics provided a good representation of the actual physical model.

The results indicate the following conclusions:

1. The geared-elevator (2.8 to 1.0 gear ratio) configuration fluttered experimentally at about 20% higher dynamic pressures than the locked-elevator (1.0 to 1.0 gear ratio) configuration. Gearing the elevator not only made the tail more efficient aerodynamically but also better from a flutter standpoint.

2. The experimental flutter boundary was nearly flat at transonic speeds (Mach numbers 0.9 to 1.1) for both configurations.

3. Comparisons of the experimental and analytical results for the geared-elevator (2.8 to 1.0 ratio) configuration indicate that the experimental flutter dynamic pressure level was best predicted by the discrete-elevator analysis, whereas both warped-surface analyses predicted somewhat lower levels. Thus, inclusion of discrete-elevator aerodynamic effects improved the correlation with experiment appreciably. However, the warped surface methods predicted more closely the experimental flutter frequencies and Mach number trends.

4. Differences in mathematical implementation of the single-warped surface analyses caused as much as a 7% difference in the predicted flutter dynamic pressures.

## References


[1]Rowe, W. S., Redman, M. C., Ehlers, F. E., and Sebastian, J. D., "Prediction of Unsteady Aerodynamic Loadings Caused by Leading Edge and Trailing Edge Control Surface Motions in Subsonic Compressible Flow — Analysis and Results," CR-2543, 1975, NASA.

[2]Redman, M. C., and Rowe, W. S., "Prediction of Unsteady Aerodynamic Loadings Caused by Leading Edge and Trailing Edge Control Surface Motions in Subsonic Compressible Flow — Computer Program Description," (The Boeing Company; NASA Contract NAS1-12020), CR-132634, 1975, NASA.

[3]Watkins, Charles E., Woolston, Donald S., and Cunningham, Herbert J., "A Systematic Kernel Function Procedure for Determining Aerodynamic Forces on Oscillating or Steady Finite Wings at Subsonic Speeds," TR R-48; 1959, NASA.

[4]Harder, Robert L., and Desmarais, Robert N., "Interpolation Using Surface Splines," Journal of Aircraft, Vol. 9, No. 2, Feb. 1972, pp. 189-191.

[5]Desmarais, Robert N., and Bennett, Robert M., "An Automated Procedure for Computing Flutter Eigenvalues," Journal of Aircraft, Vol. 11, No. 2, Feb. 1974, pp. 75-80.

TABLE 1. NATURAL VIBRATION FREQUENCIES AND DAMPINGS OF MODEL CONFIGURATIONS

Note: The flutter analysis of the model with gear ratio 2.8 to 1.0 employed measured frequencies and calculated mode shapes

| Mode | Gear ratio: 2.8 to 1.0 | | | Gear ratio: 1.0 to 1.0 | |
|---|---|---|---|---|---|
| | Calculated | Measured | | Measured | |
| | Hz | Hz | g | Hz | g |
| Sting* | | 1.9 | - | 1.9 | - |
| 1 | 7.5 | 7.0 | 0.012 | 7.3 | 0.017 |
| Sting body* | - | 15.4 | .008 | 15.5 | .011 |
| 2 | 19.6 | 21.1 | .028 | 24.4 | .018 |
| 3 | 30.9 | 32.0 | .024 | 32.5 | .023 |
| 4 | 45.4 | 46.5 | .012 | 47.7 | .014 |
| 5 | 47.9 | 47.9 | .023 | 60.9 | .013 |
| 6 | 66.3 | 66.9 | .014 | 69.8 | .013 |

*Not included in flutter analyses.

TABLE 2. EXPERIMENTAL FLUTTER RESULTS

| Mach number | Dynamic pressure, kPa | Velocity, m/sec | Density, $kg/m^3$ | Flutter frequency, Hz |
|---|---|---|---|---|
| Elevator gear ratio 2.8 to 1.0 | | | | |
| 0.706 | 14.63 | 110.6 | 1.3939 | 11.6 |
| .872 | 12.49 | 136.0 | 1.3513 | 10.6 |
| .982 | 12.29 | 152.5 | 1.0570 | 10.5 |
| 1.131 | 12.19 | 173.7 | 0.8076 | 10.0 |
| Elevator gear ratio 1.0 to 1.0 | | | | |
| 0.884 | 10.27 | 137.0 | 1.0941 | 9.6 |
| 1.006 | 10.29 | 154.9 | 0.8581 | 9.5 |
| 1.140 | 10.22 | 173.9 | .6757 | 9.4 |

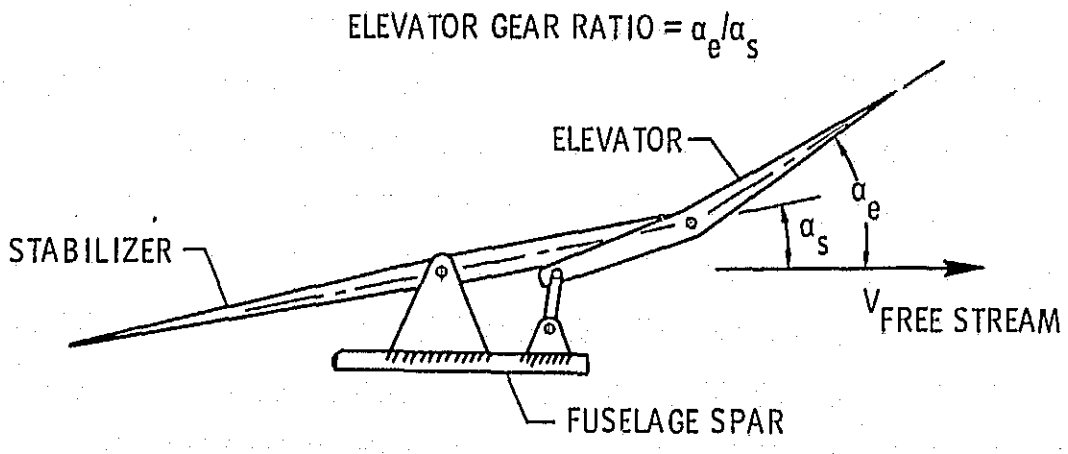


Figure 1. Schematic of elevator-gearing arrangement.

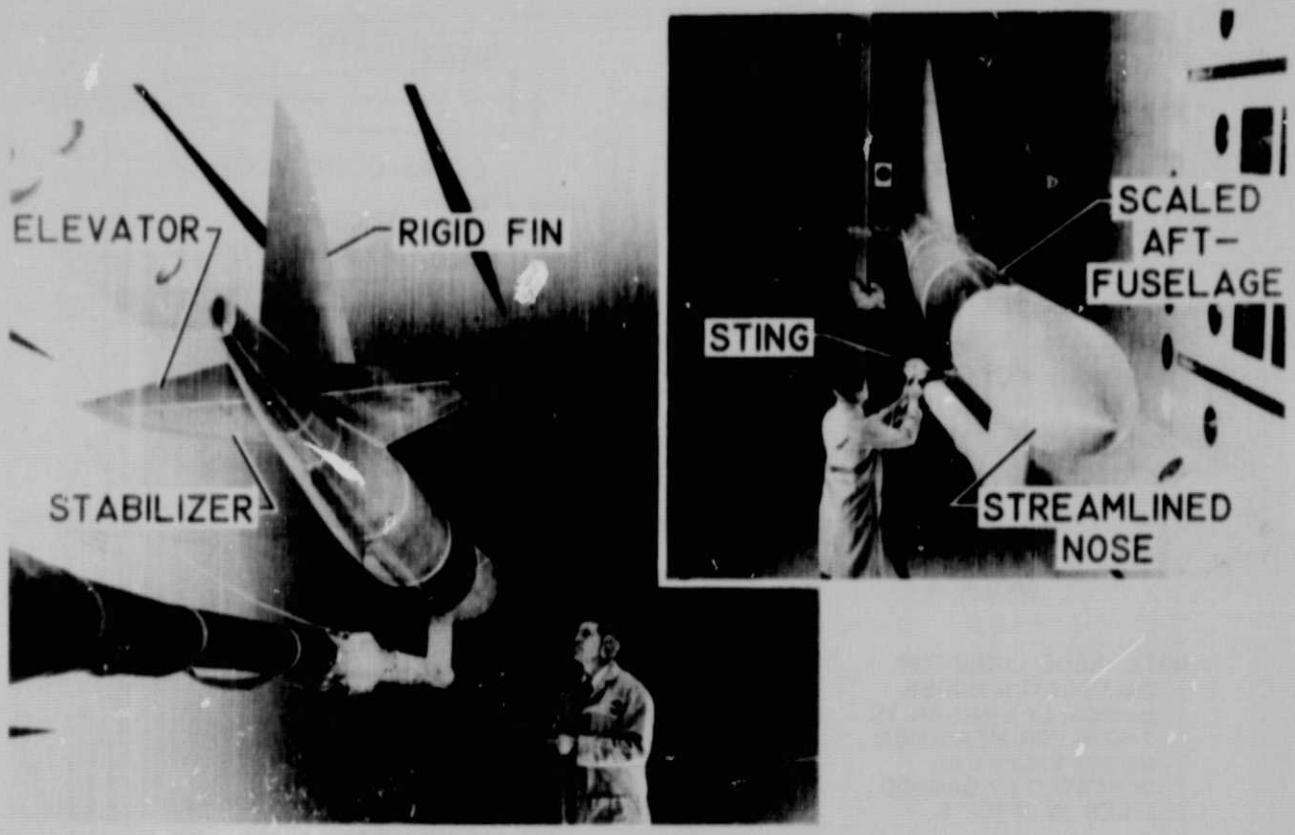


Figure 2. Photographs of model in wind tunnel.

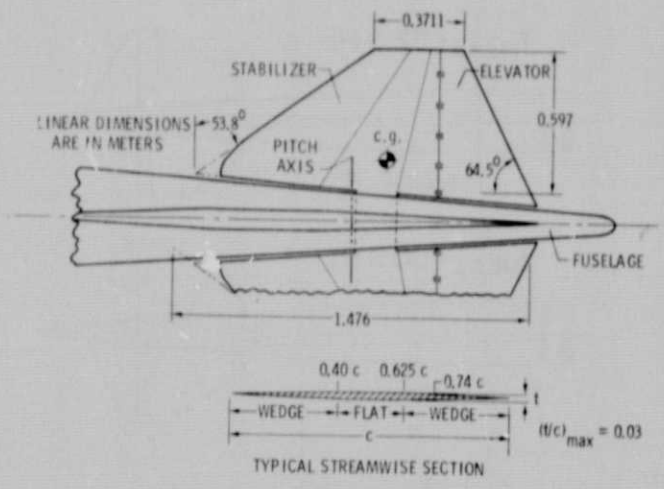


Figure 3. Sketch of horizontal-tail model.

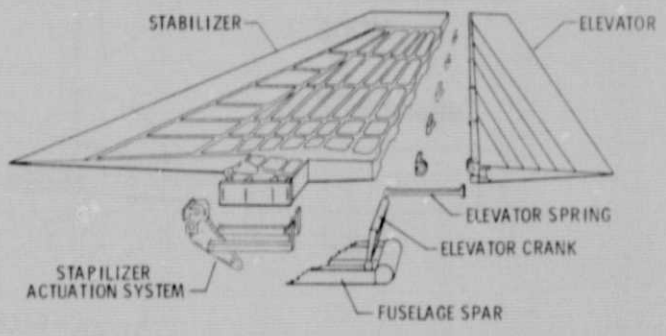


Figure 4. Sketch showing horizontal-tail model construction details.

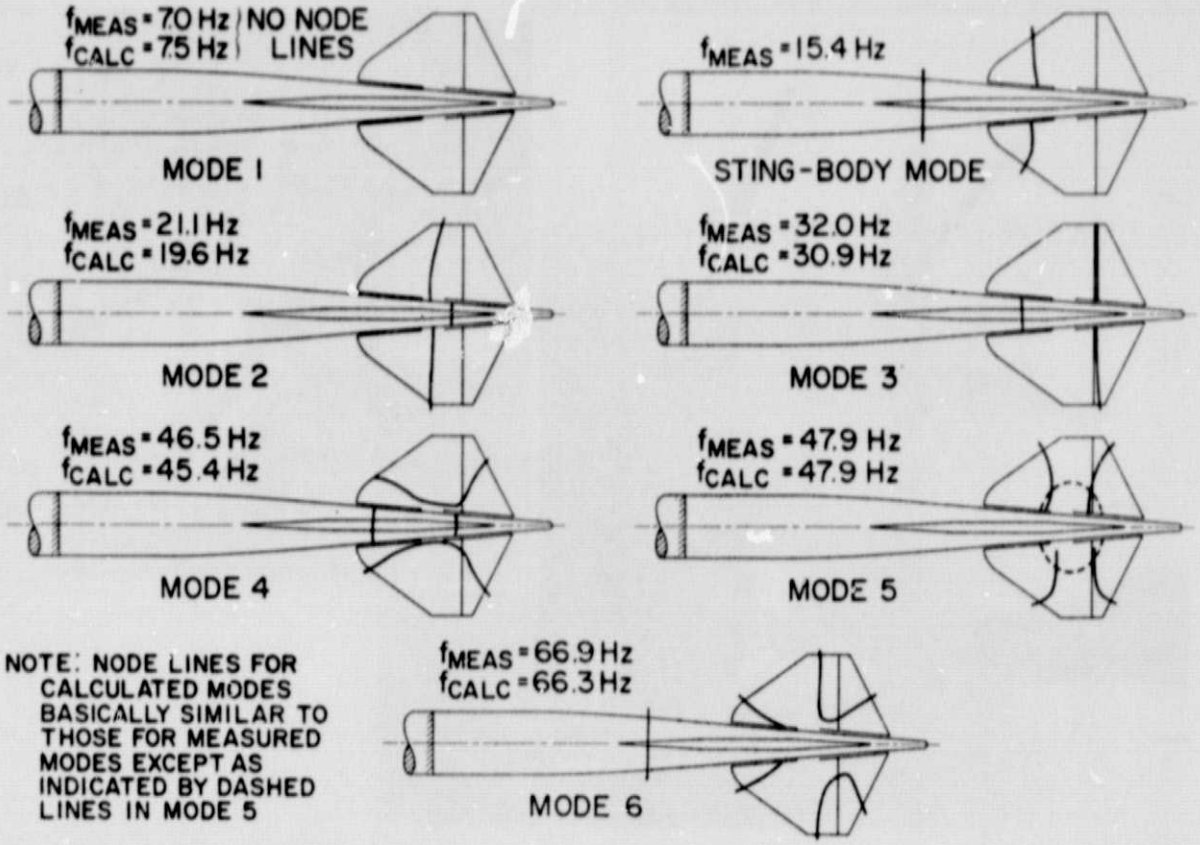


Figure 5. Measured and calculated node lines and frequencies of symmetric natural vibration modes for geared-elevator (2.8 to 1.0 gear ratio) configuration.

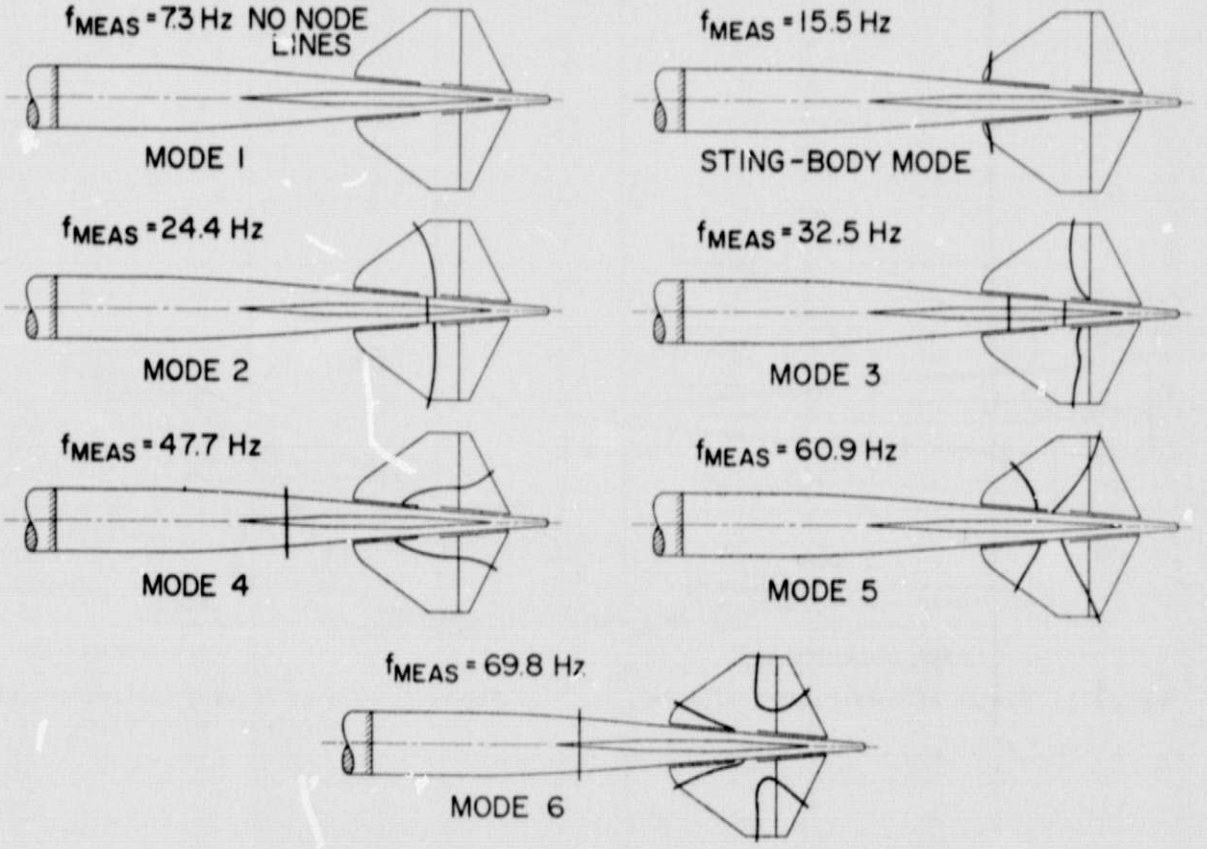


Figure 6. Measured node lines and frequencies of symmetric natural vibration modes for locked-elevator (1.0 to 1.0 gear ratio) configuration.

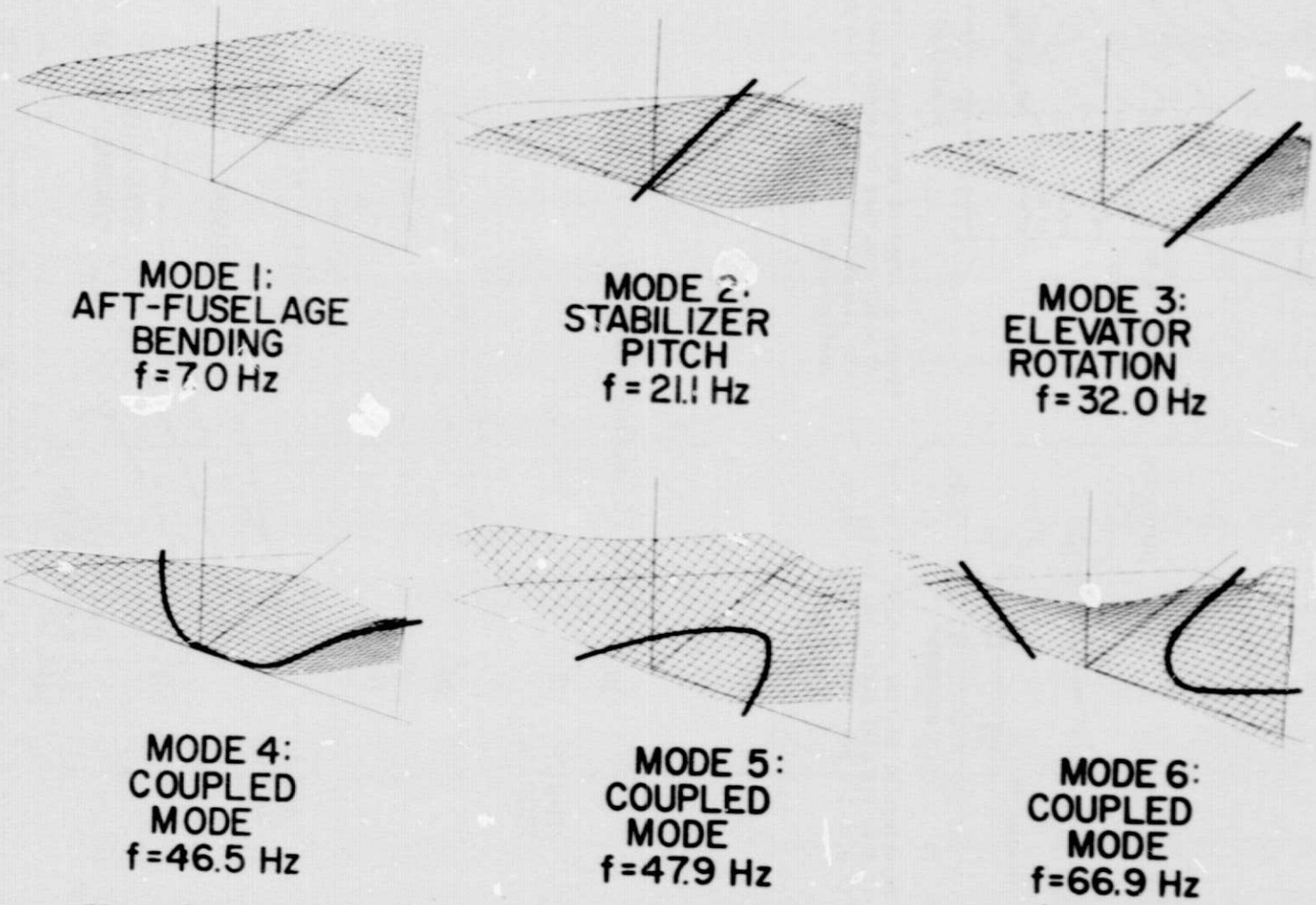


Figure 7. Isometric projections of stabilizer-elevator portions of calculated mode shapes (2.8 to 1.0 gear ratio).

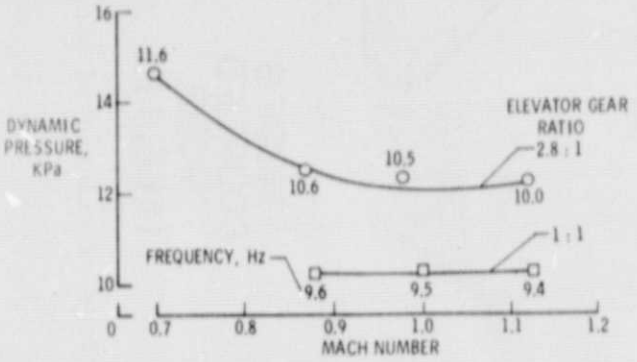


Figure 8. Experimental flutter results for geared-elevator (2.8 to 1.0 gear ratio) and locked-elevator (1.0 to 1.0 gear ratio) configuration.

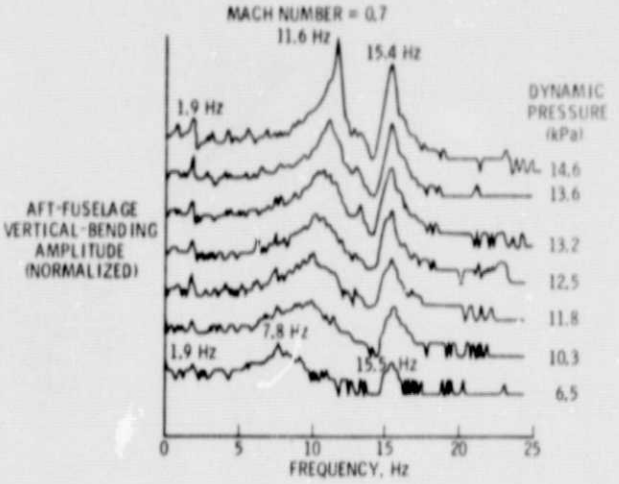


Figure 9. Typical experimental frequency spectra of model response to random tunnel turbulence for the geared-elevator (2.8 to 1.0 gear ratio) configuration.

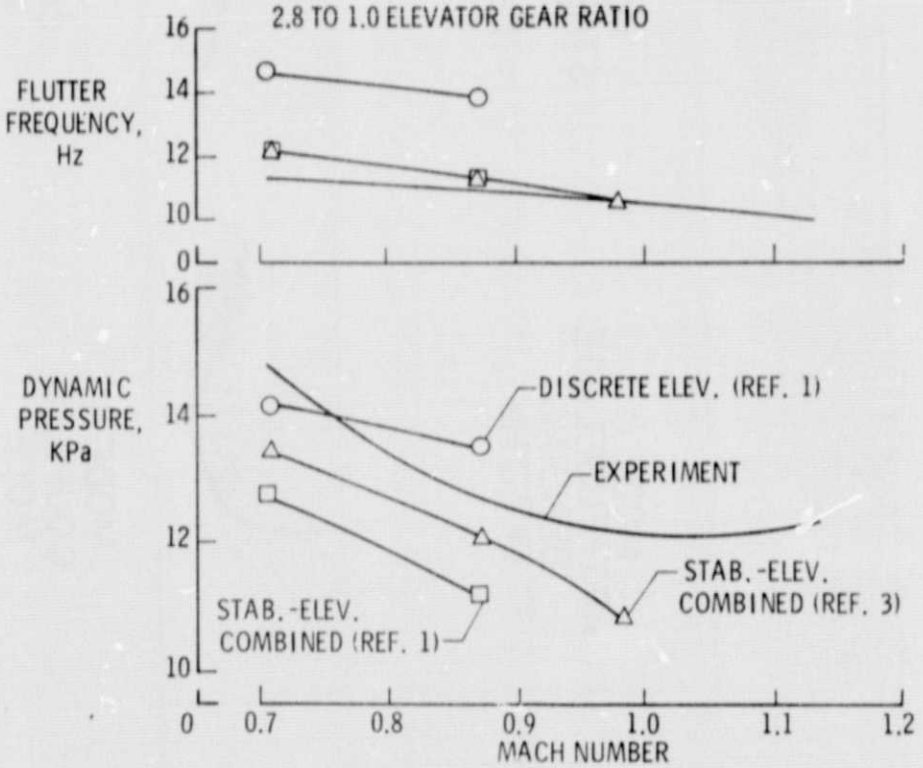


Figure 10. Comparison of calculated and experimental flutter results for geared-elevator (2.8 to 1.0 gear ratio) configuration.